Electronic Supplementary Information

Boosting hydrazine oxidation and hydrogen evolution catalysis with anchored Ru clusters by electronically tunable Ru-S-C Bonds

Huaikun Zhang[a,#], Wentao Wang[b,#], Zechuan Dai[a], Yin Zhu[a], Mingyu Cheng[a], Bocheng Zhang[a], Yafei Feng[a], Yangyang Zhang[a] and Genqiang Zhang,[a,*]

[a] Hefei National Research Center for Physical Sciences at the Microscale, CAS Key Laboratory of Materials for Energy Conversion, Department of Materials Science and Engineering, University of Science and Technology of China Hefei, Anhui 230026, China

[b] Guizhou Provincial Key Laboratory of Computational Nano-Material Science, Guizhou Education University, Guiyang, Guizhou 550018, China

[#] These two authors contribute equally to this work.

Corresponding Author:

G. Q. Zhang, E-mail: gqzhangmse@ustc.edu.cn

Computational details.

Density functional theory (DFT) based first-principles calculations are performed using the projected augmented wave (PAW)[1] method implemented in the Vienna *ab initio* simulation package (VASP).[2,3] The Kohn-Sham one-electron states are expanded using the plane-wave basis set with a kinetic energy cutoff of 500 eV. The Perdew-Burke-Ernzerhof (PBE)[4] exchange-correlation functional within the generalized gradient approximation (GGA) is employed. To study the adsorption of the Ru cluster on graphene involved in HER and HzOR, we have considered the Ru19 cluster[5] adsorbed onto a periodic 7 × 7 supercell of graphene with 98 carbon atoms (Ru19-graphene). In this Ru19- graphene model, the two N atoms substitute two of the graphene C and two S atoms substitute two of the graphene C to model the 2SN: Ru19-graphene, as shown in Fig. 6A. The Brillouin-zone (BZ) integration is carried out using the Monkhorst-Pack[6] sampling method with a density of 2×2×1 for the geometry optimizations. A sufficiently large vacuum region of 20 Å was used for all the systems to ensure the periodic images to be well separated. During the geometry optimizations, all the atoms are allowed to relax until the maximum magnitude of the force acting on the atoms is smaller than 0.03 eV/Å, and the total energy convergence criterion is set to 1×10^{-4} eV. The calculation of the Gibbs free energy of the intermediates followed the Nørskov method.[7]

The oxidation of hydrazine into nitrogen and hydrogen occurs in the following six consecutive elementary steps:

(A) $* + N_2H_4 \rightarrow *N_2H_4$, Eq. (1)

(B) $*N_2H_4 \rightarrow *N_2H_3 + H^+ + e^-$, Eq. (2)

(C) $*N_2H_3 \rightarrow *N_2H_2 + H^+ + e^-$, Eq. (3)

(D) $*N_2H_2 \rightarrow *N_2H + H^+ + e^-$, Eq. (4)

(E) $*N_2H \rightarrow *N_2 + H^+ + e^-$, Eq. (5)

(F) $*N_2 \rightarrow * + N_2$. Eq. (6)

The asterisk (*) represents the reaction surface of Ru19- graphene and 2SN: Ru19-graphene. "$*N_2H_4$", "N_2H_3", "N_2H_2", "N_2H", and "$*N_2$" denote the models with the corresponding chemisorbed species residing in the reaction surfaces. Among these six elementary steps, steps (A) and (F) are the adsorption of N_2H_4 and desorption of N_2, respectively. The other four elementary steps involve the generation of one proton and

one electron. Then, using the computational hydrogen electrode (pH = 0, p = 1 atm, T = 298 K),[7] the Gibbs free energy of $H^+ + e^-$ was replaced implicitly with the Gibbs free energy of one-half an H_2 molecule. Thus the reaction Gibbs free energies can be calculated with Eqs: [8-11]

$$\Delta G_A = G_{*N_2H_4} - G_* - G_{N_2H_4} \quad \text{Eq. (7)}$$

$$\Delta G_B = G_{*N_2H_3} + 0.5G_{H_2} - G_{*N_2H_4} - eU - kT\ln 10 \times pH \quad \text{Eq. (8)}$$

$$\Delta G_C = G_{*N_2H_2} + 0.5G_{H_2} - G_{*N_2H_3} - eU - kT\ln 10 \times pH \quad \text{Eq. (9)}$$

$$\Delta G_D = G_{*N_2H} + 0.5G_{H_2} - G_{*N_2H_2} - eU - kT\ln 10 \times pH \quad \text{Eq. (10)}$$

$$\Delta G_E = G_{*N_2} + 0.5G_{H_2} - G_{*N_2H} - eU - kT\ln 10 \times pH \quad \text{Eq. (11)}$$

$$\Delta G_F = G_* + G_{N_2} - G_{*N_2} \quad \text{Eq. (12)}$$

U and the pH value in this work are set to zero. The adsorption or reaction Gibbs free energy is defined as $\triangle G = \Delta E + (ZPE - T\triangle S)$, where ΔE is the adsorption or reaction energy based on DFT calculations. ΔZPE is the zero-point energy (ZPE) correction, T is the temperature, and ΔS is the entropy change. For each system, its ZPE can be calculated by summing vibrational frequencies overall normal modes ν ($ZPE = 1/2\Sigma\hbar\nu$). The entropies of gas-phase H_2, N_2, and NH_2NH_2 are obtained from the NIST database[12] with the standard condition, and the adsorbed species were only taken vibrational entropy (Sv) into account, as shown in the following formula:

$$S_V = \sum_i R\left\{\frac{h\nu_i}{k_B T}\left[\exp\left(\frac{h\nu_i}{k_B T}\right) - 1\right]^{-1} - \ln\left[1 - \exp\left(-\frac{h\nu_i}{k_B T}\right)\right]\right\} \quad \text{Eq. (13)}$$

Among which $R = 8.314\ J\cdot mol^{-1}\cdot K^{-1}$, $T = 298.15\ K$, $h = 6.63 \times 10^{-34}\ J\cdot s$, $k_B = 1.38 \times 10^{-23}\ J\cdot K^{-1}$, i is the frequency number, ν_i is the vibrational frequency (unit is cm^{-1}).

Under the standard condition, the overall HER pathway includes two steps: first, adsorption of hydrogen on the catalytic site (*) from the initial state ($H^+ + e^- + *$), second, release the product hydrogen ($1/2H_2$). Therefore, the Gibbs free energy of the adsorption of the intermediate hydrogen on a catalyst (ΔG_H) is the key descriptor of the HER activity of the catalyst and is obtained by:

$$\Delta G_H = \Delta E_H + \Delta ZPE - T\Delta S \quad \text{Eq. (14)}$$

where ΔE_H, ΔZPE and ΔS are the adsorption energy, zero-point energy change and entropy change of H adsorption, respectively. The charge transfer between N_2H_4

dehydrogenation intermediate ("*N_2H_4", "*N_2H_3", "*N_2H_2", "*N_2H", and "*N_2") adsorbing the 2SN: Ru19-graphene interface (Ru19 cluster) is estimated by employing the Bader Charge Analysis version 1.03.[13,14]

The charge density difference ($\Delta\rho$) was obtained using the following equation: $\Delta\rho = \rho(\text{surface} + \text{intermediate}) - \rho(\text{surface}) - \rho(\text{intermediate})$. Where ρ (surface + intermediate), ρ(surface) and ρ(intermediate) are the total charge density of the N_2H_4 dehydrogenation intermediate ("*N_2H_4", "*N_2H_3", "*N_2H_2", "*N_2H", and "*N_2") adsorbed the 2NS: Ru19-graphene interface (Ru19 cluster), and N_2H_4 dehydrogenation intermediate ("*N_2H_4", "*N_2H_3", "*N_2H_2", "*N_2H", and "*N_2"), respectively. The charge density difference quantifies the redistribution of electron charge due to the interaction between N_2H_4 dehydrogenation intermediate ("*N_2H_4", "*N_2H_3", "*N_2H_2", "*N_2H", and "*N_2") and the 2NS: Ru19-graphene interface (Ru19 cluster) of both the two samples.

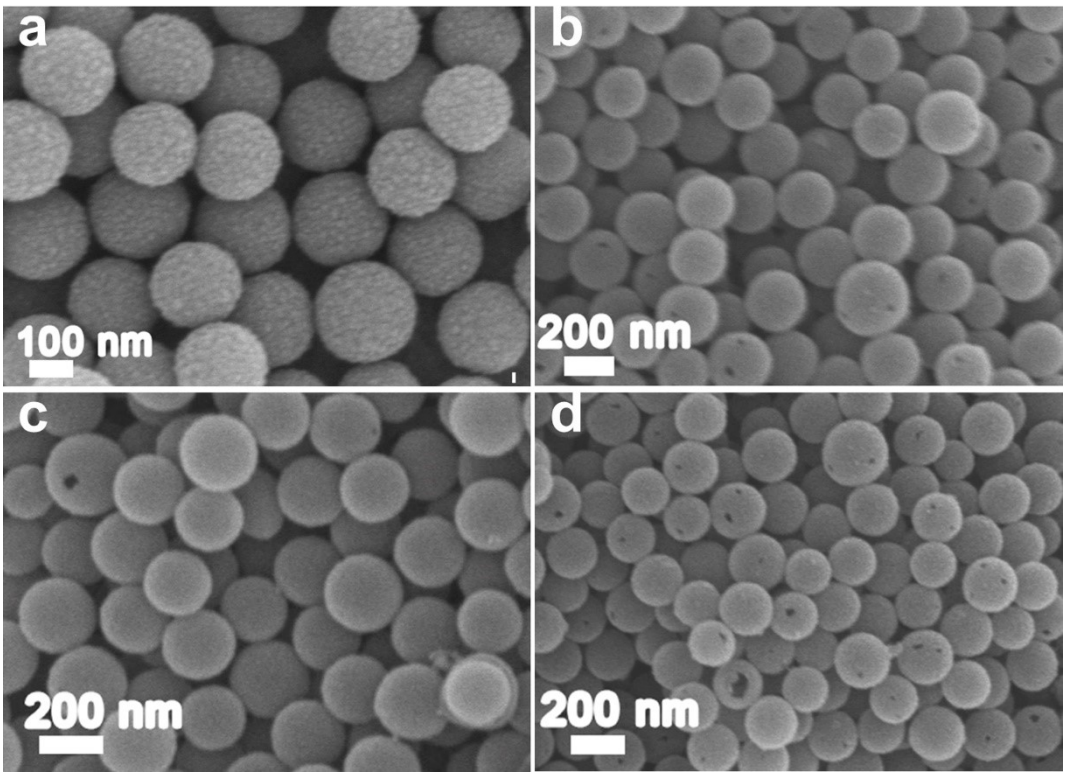

Figure S1. The SEM images of different intermediates. (a) RF/SiO_2; (b) HCS; (c) NSCS; (d) Ru/NSCS-pre.

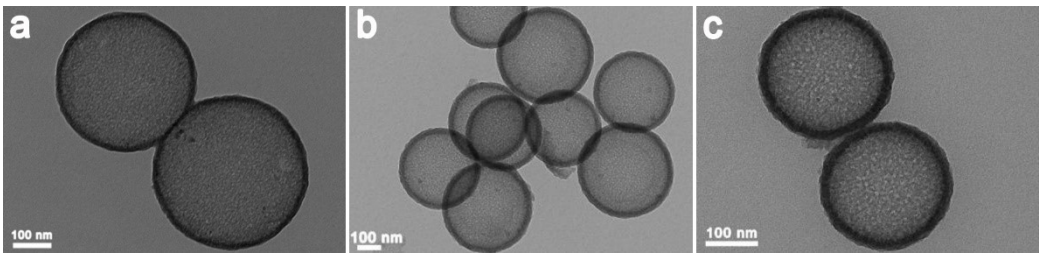

Figure S2. The TEM images of different intermediates. (a) HCS; (b) NSCS; (c) Ru/NSCS-pre.

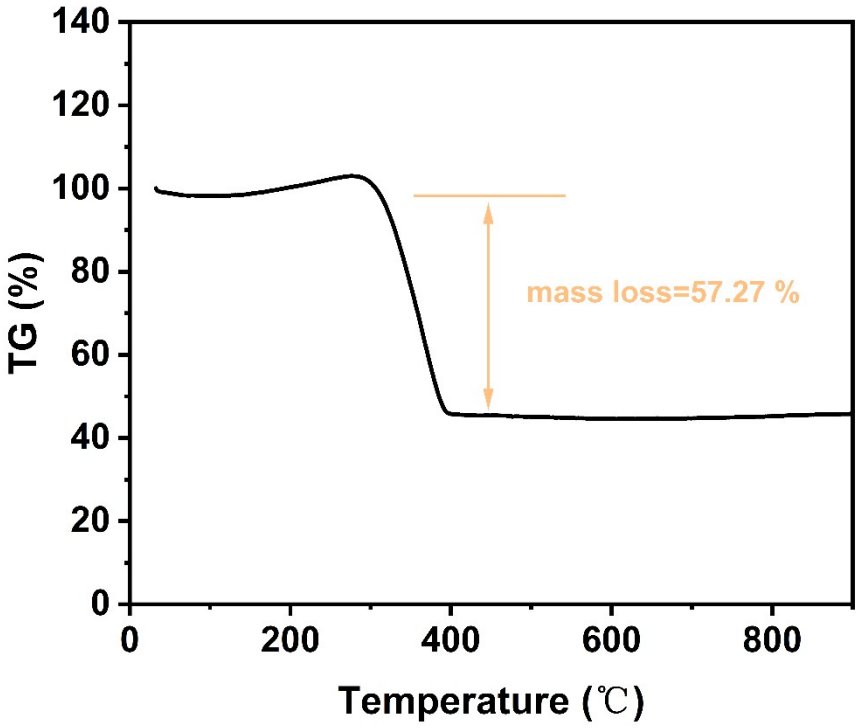

Figure S3. The Thermogravimetric Analysis results of Ru/NSCS.

Ru/NSCS materials will be transformed into RuO_2 after heat treatment in the air. The mass percentage of Ru can be calculated according to the following formula using the mass loss percentage:

$$W = (1 - a) * \frac{M(Ru)}{M(RuO_2)}$$

W is the mass percentage of Ru; a stands for percentage of mass loss; $M(Ru)$ and $M(RuO_2)$ represent the relative molecular weights of Ru and RuO_2, respectively. By substituting relevant data into the above equation, the content of Ru can be obtained as 32.4 wt %.

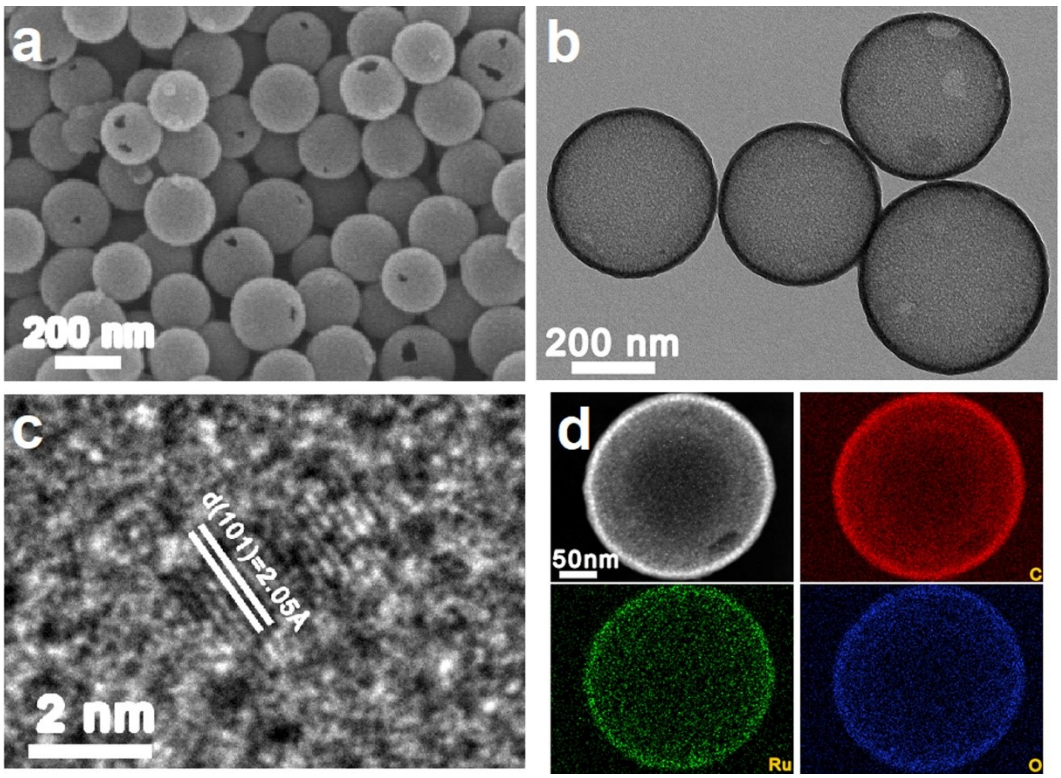

Figure S4. Structural characterizations of the Ru/CS. (a) SEM; (b) TEM; (c~d) HRTEM images and corresponding elemental mappings.

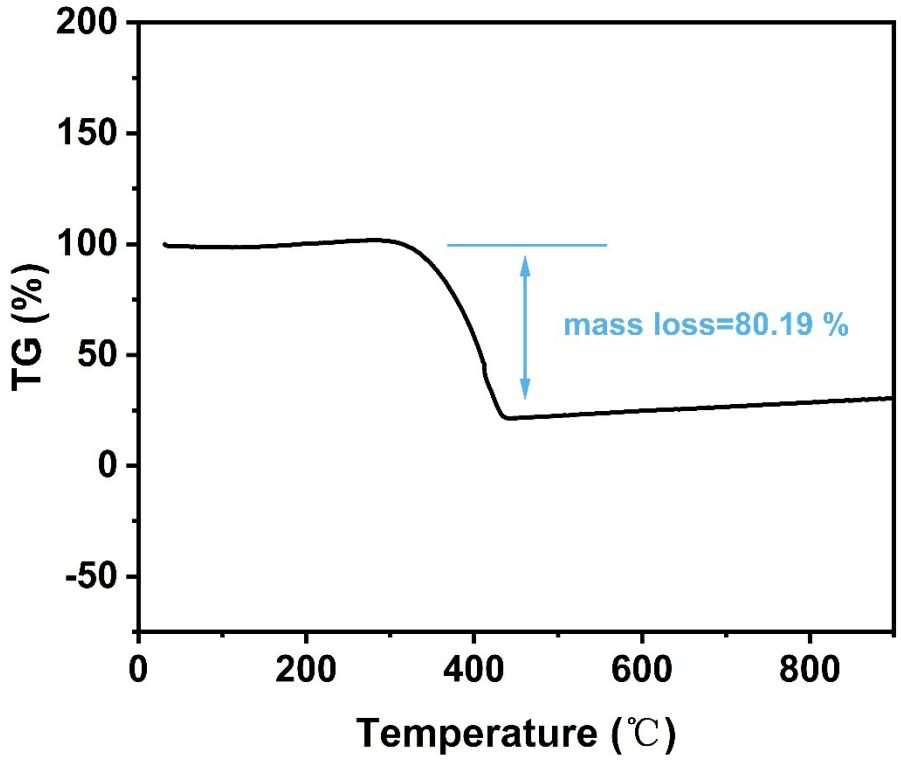

Figure S5. The Thermogravimetric Analysis results of Ru/CS.

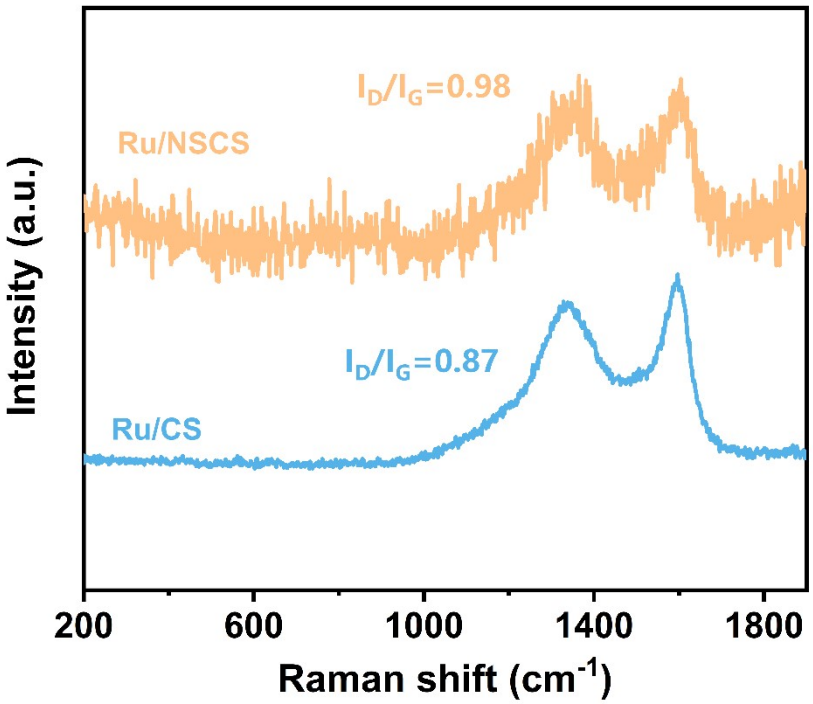

Figure S6. Raman spectra of Ru/NSCS and Ru/CS.

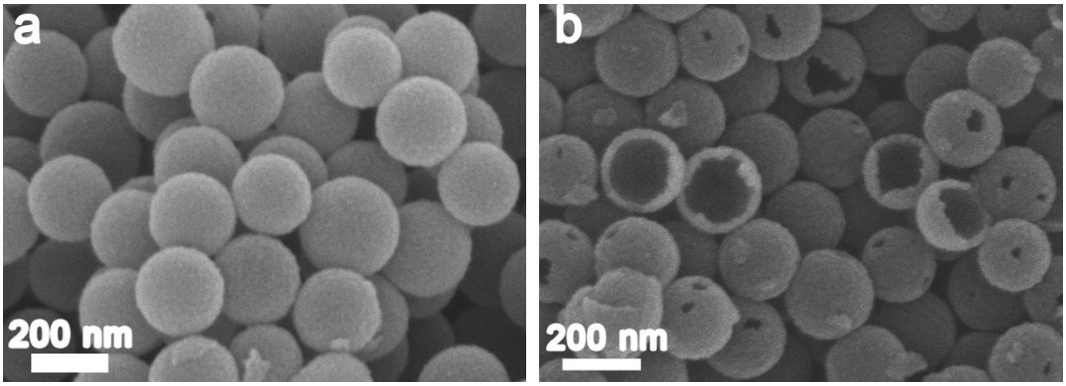

Figure S7. The SEM images of (a) Ru/NSCS-4 and (b) Ru/NSCS-12.

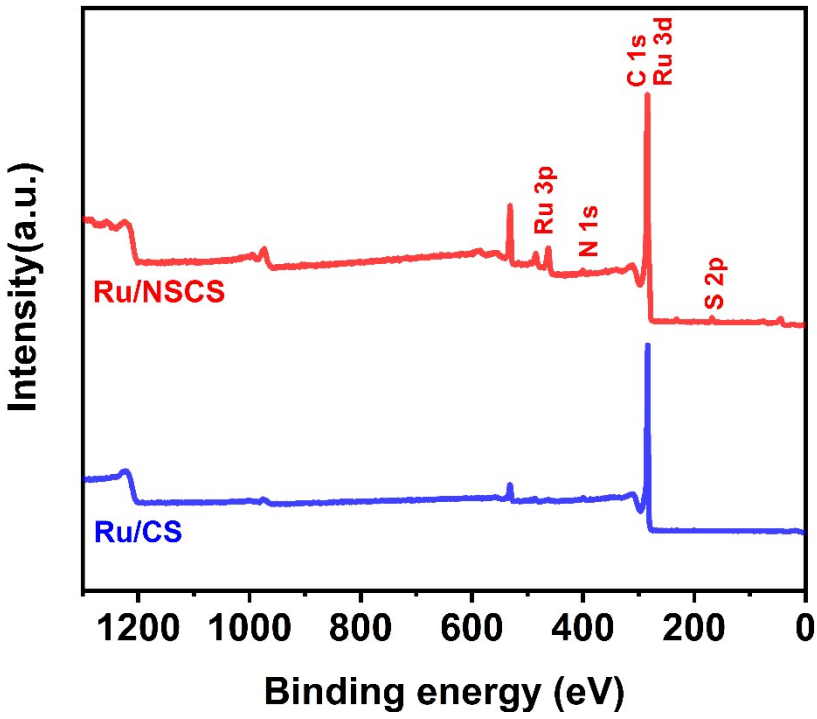

Figure S8. XPS survey spectra of Ru/NSCS and Ru/CS.

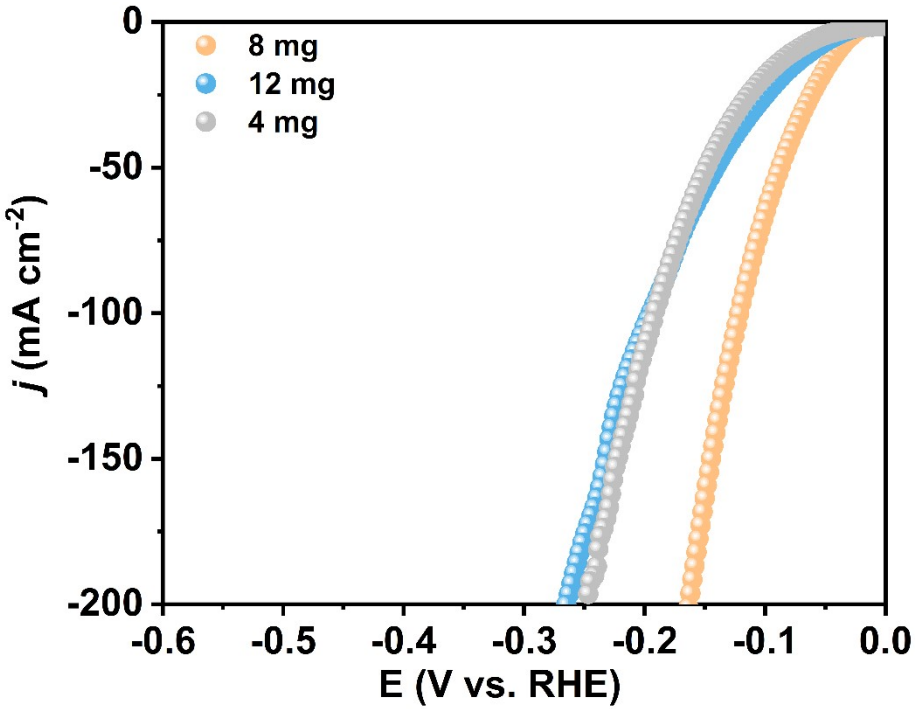

Figure S9. The study of HER performances of Ru/NSCS-4, Ru/NSCS-8 and Ru/NSCS-12. The LSV curves obtained in 1 M KOH without IR correction.

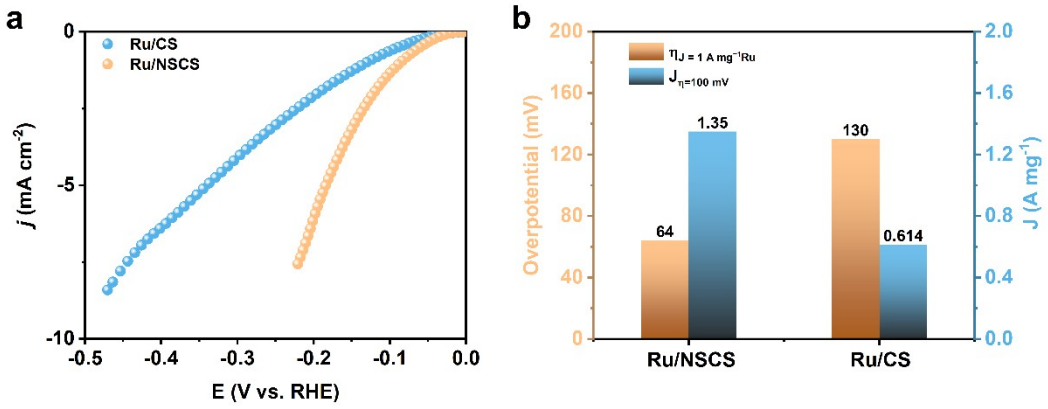

Figure S10. Mass activity of Ru/NSCS and Ru/CS for HER measured in 1.0 M KOH. (a) LSV curves; (b) the compared working potential at 1 A mg^{-1} Ru and mass current density at 100 mV.

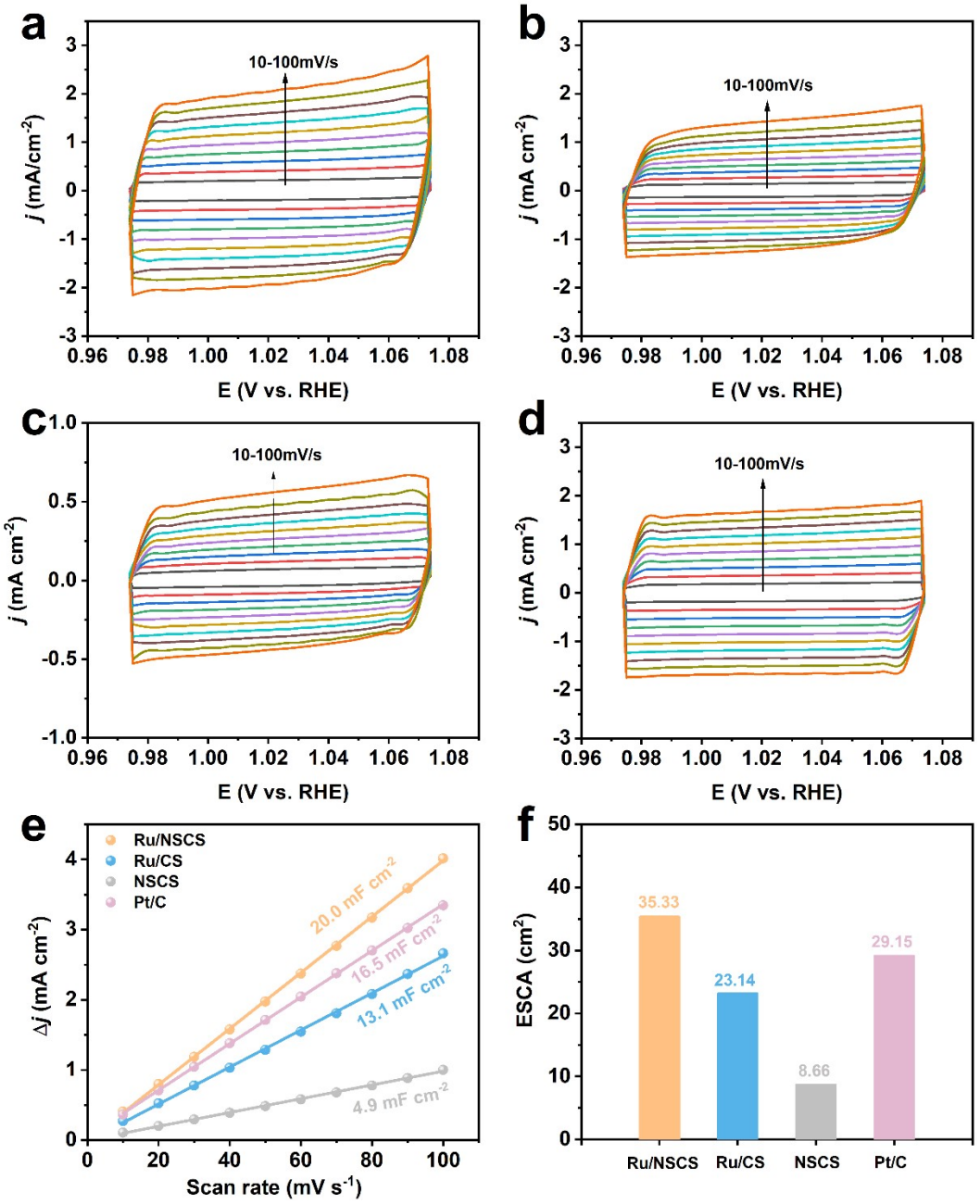

Figure S11. The evaluation of ECSA. The CV curves of (a) Ru/NSCS, (b) Ru/CS, (c)NSCS, and (d) Pt/C with the scan rate ranging from 10 to 100 mV s^{-1} in 1 M KOH; (e) C_{dl} values at potential of 1.02 V (vs. RHE) and (f) ECSA values on the GCE (0.07065 cm^{-2}) for Ru/NSCS, Ru/CS, NSCS, and Pt/C.

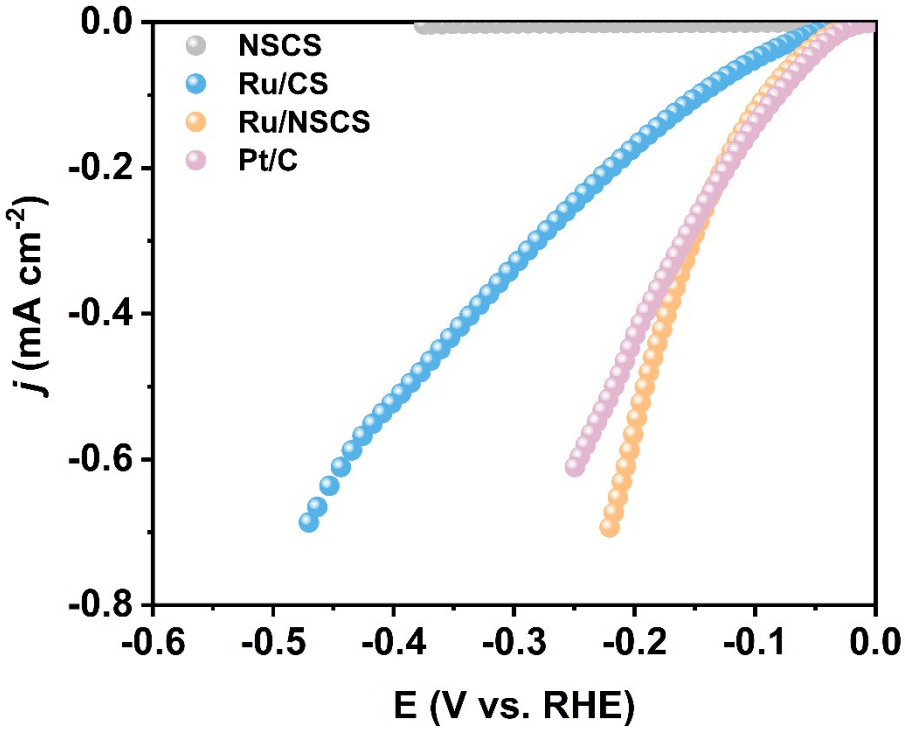

Figure S12. ECSA normalized LSV curves for HER in 1.0 M KOH.

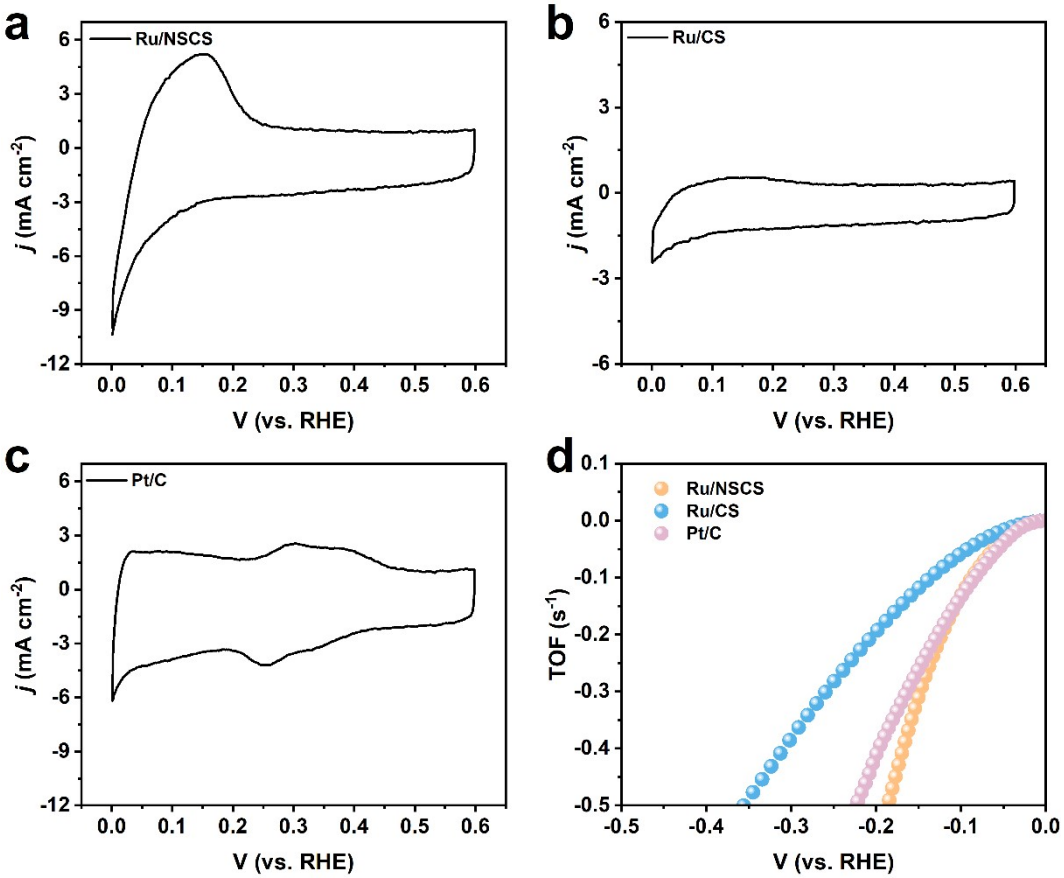

Figure S13. CV curves of different catalysts in 1.0 M KOH. (a) Ru/NSCS, (b) Ru/CS, (c) Pt/C, and (d) the corresponding TOF. The Q_s values of Ru/NSCS, Ru/CS, and Pt/C are calculated to be 0.235, 0.143, and 0.216 C cm^{-2}.

TOF is calculated according to the following formula: TOF = J/2Fn, where the "J" is the current density under certain overpotential during the HER process, the "F" is the Faraday constant (96485 C mol^{-1}) and the "n" is the mole number of the active metal sites (mol cm^{-2}). The factor 1/2 is presented because two electrons are required to form one hydrogen molecule. The n values can be obtained by cyclic voltammetry (CV) which are performed in the potential range of 0-0.6 V (vs. RHE) with a fixed scan rate of 50 mV s^{-1}. Then, by integrating the charge of each CV curve over the whole potential range, the half value of the charge is the value of the surface charge density (Q_s). Finally, the n value is computed by $n = Q_s / F$.

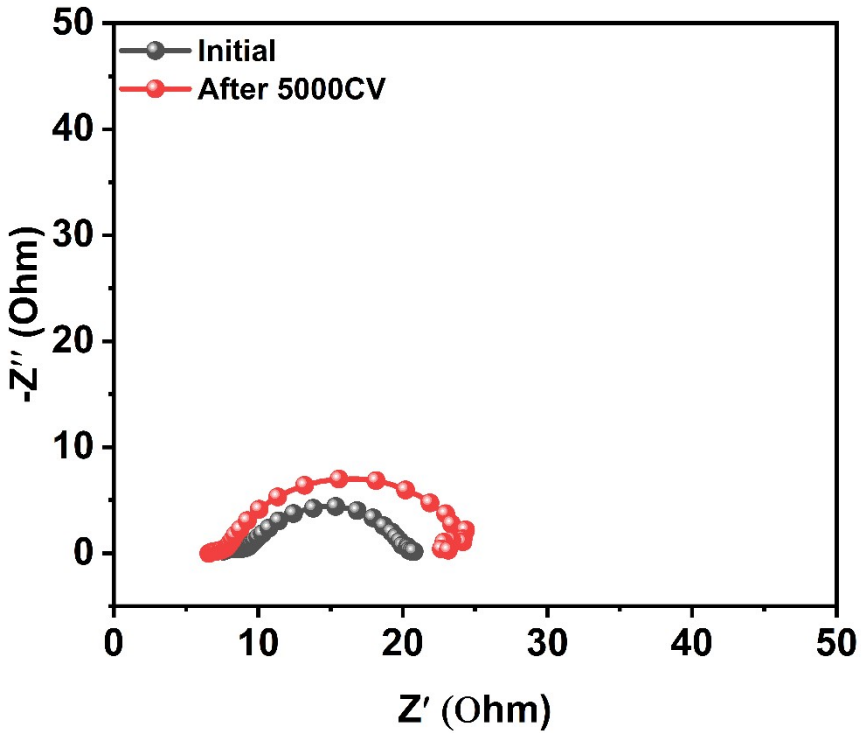

Figure S14. The compared Nyquist plots for Ru/NSCS after durability investigation. The Nyquist plots was measured at -0.1 V vs. RHE for HER.

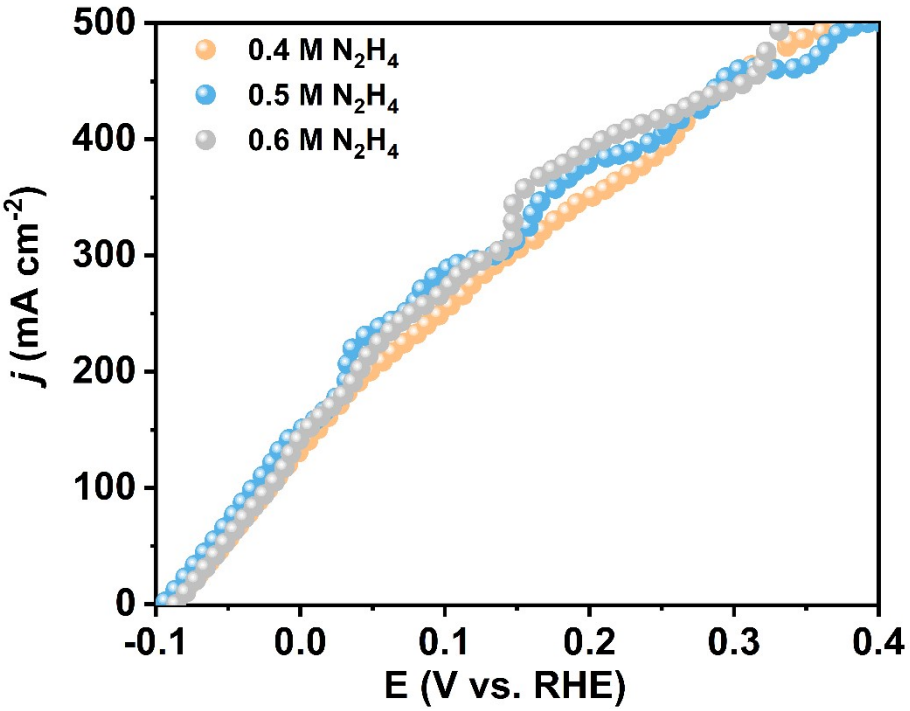

Figure S15. The LSV curves of Ru/NSCS with a scan rate of 5 mV s^{-1} in 1.0 M KOH with high concentrations of hydrazine.

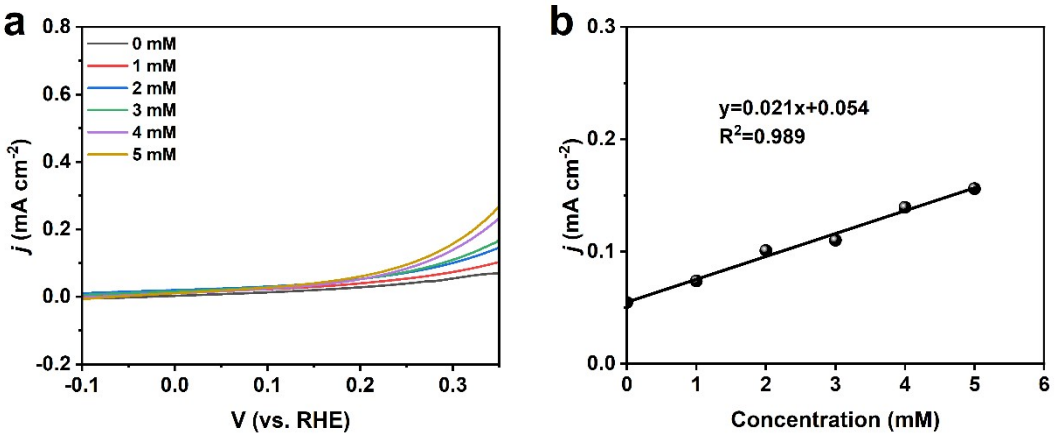

Figure S16. The electrochemical behaviors of Ru/NSCS towards the low concentrations of hydrazine. (a) The LSV curves of Ru/NSCS with a scan rate of 5 mV s^{-1} in 1.0 M KOH with the concentrations of hydrazine from 0 to 5 mM; (b) the corresponding calibration curve at potential of 0.3 V.

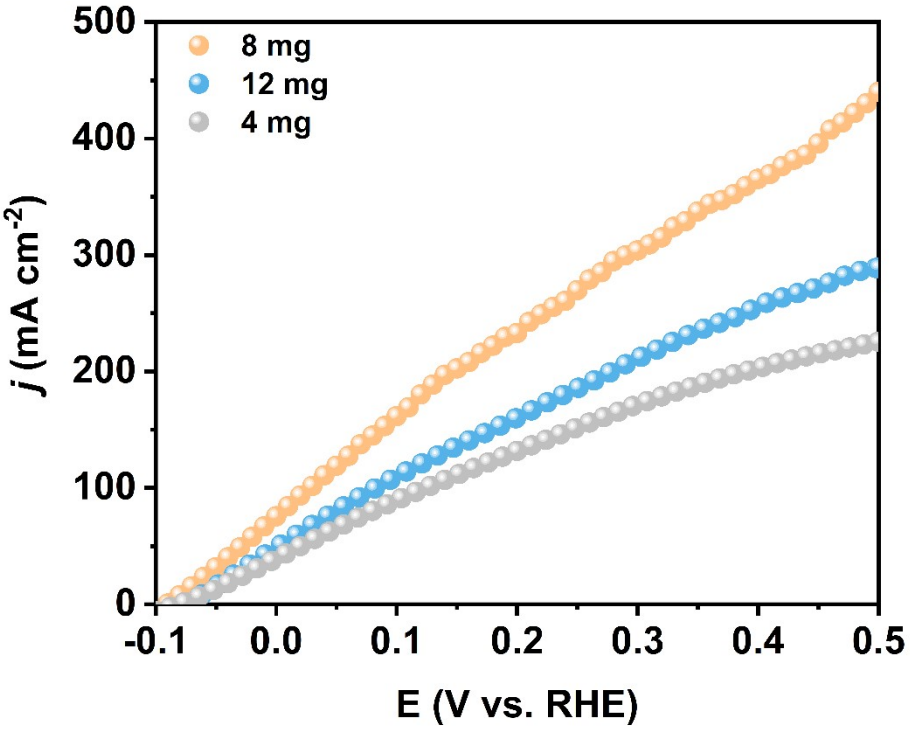

Figure S17. The study of HzOR performances of Ru/NSCS-4, Ru/NSCS-8 and Ru/NSCS-12. The LSV curves is obtained in 1 M KOH/0.4 M N_2H_4 without IR-corrected.

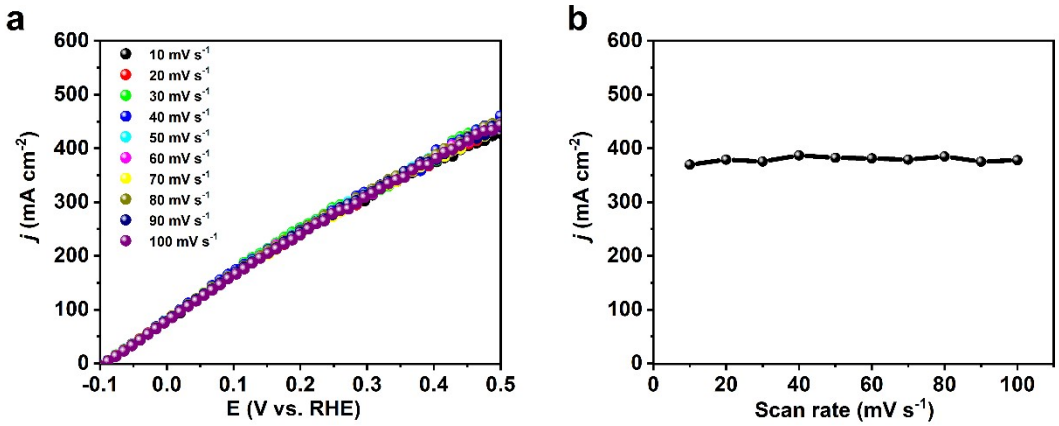

Figure S18. LSV curves of Ru/NSCS at different scan rates in 1 M KOH/0.4 M N_2H_4. (a) LSV curves; (b) Current density contrast at 0.4 V vs. RHE.

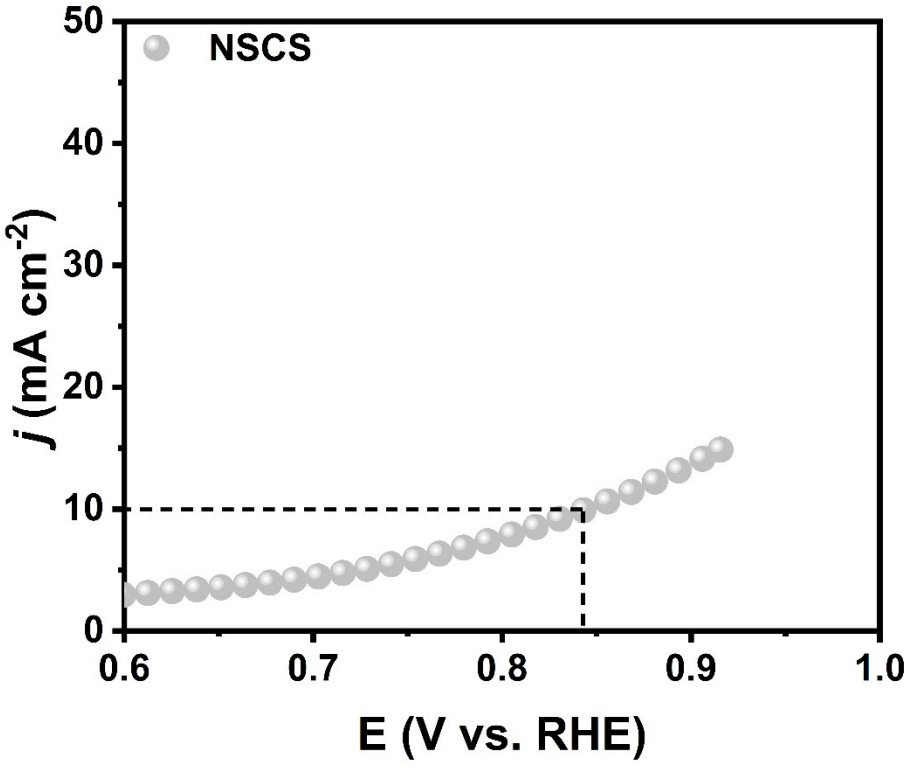

Figure S19. LSV curves of NSCS at high potential in 1 M KOH/0.4 M N_2H_4.

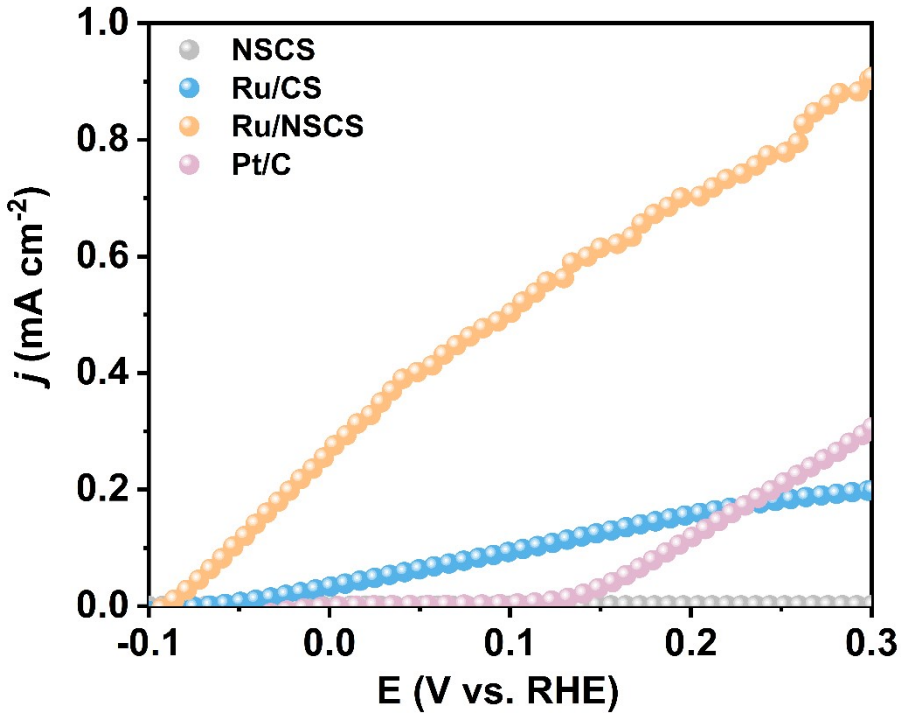

Figure S20. ECSA normalized LSV curves for HzOR in 1.0 M KOH/0.4 M N_2H_4.

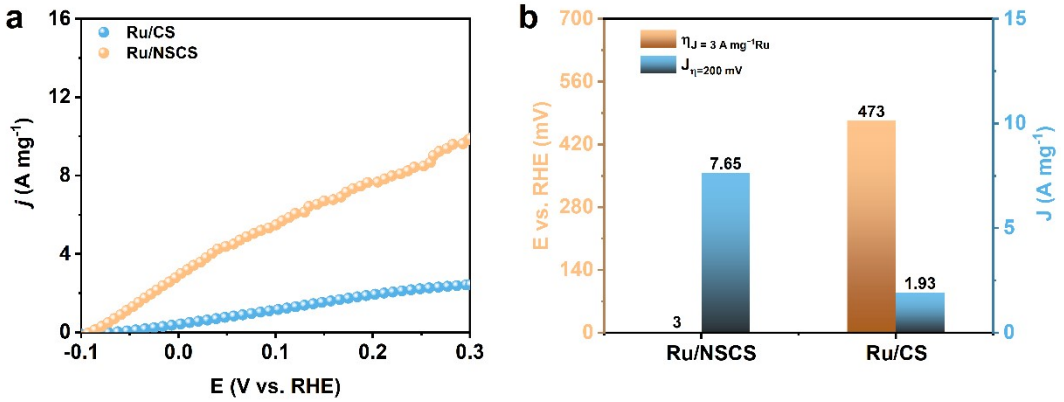

Figure S21. Mass activity of Ru/NSCS and Ru/CS for HzOR measured in 1.0 M KOH/0.4 M N_2H_4. (a) LSV curves; (b) The compared working potential at 3 A mg^{-1} Ru and mass current density at 200 mV.

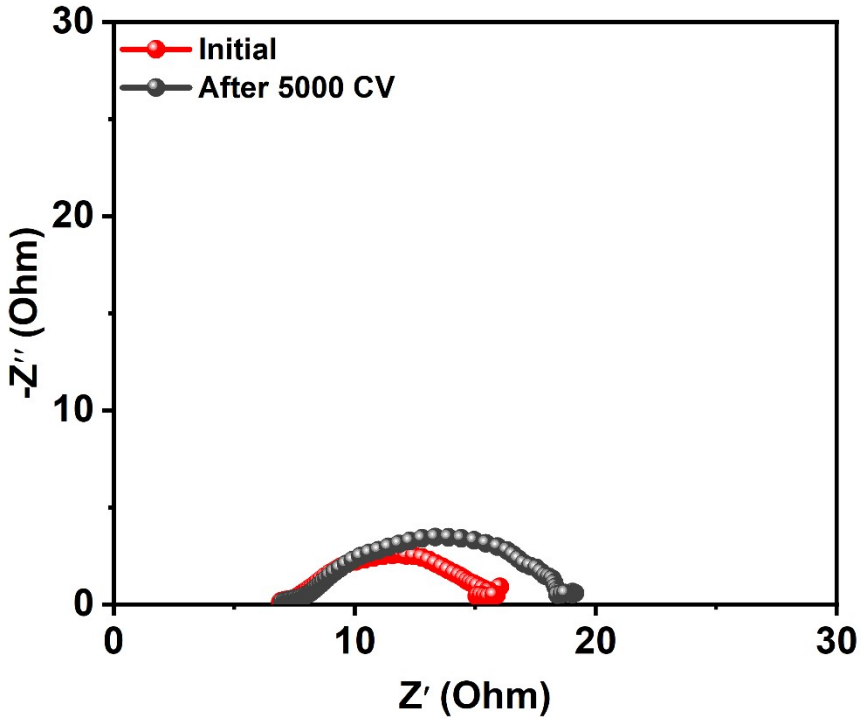

Figure S22. The compared Nyquist plots for Ru/NSCS after durability investigation. The Nyquist plots was measured at -0.05 V vs. RHE for HzOR.

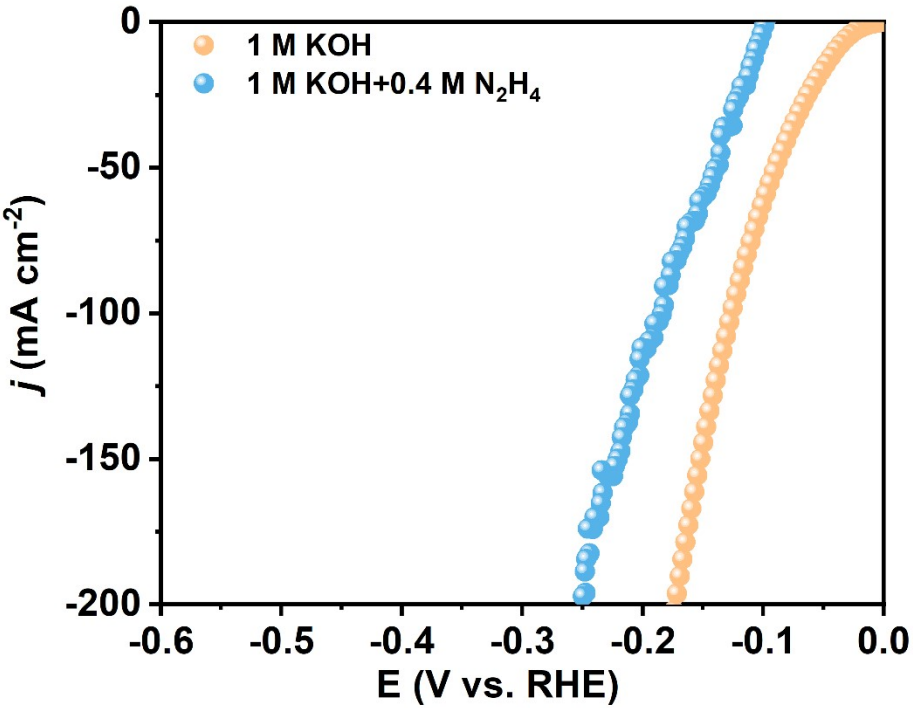

Figure S23. The LSV curves of Ru/NSCS for HER in 1 M KOH with and without hydrazine.

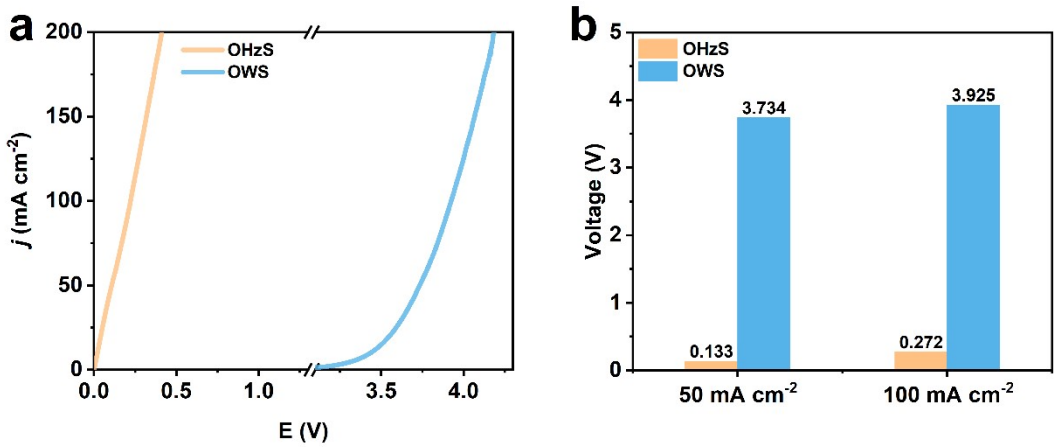

Figure S24. The comparison of Ru/NSCS for OWS and OHzS performance. (a) LSV curves of OHzS and OWS; (b) Potential contrast at 50 and 100 mA cm^{-2} of OHzS and OWS.

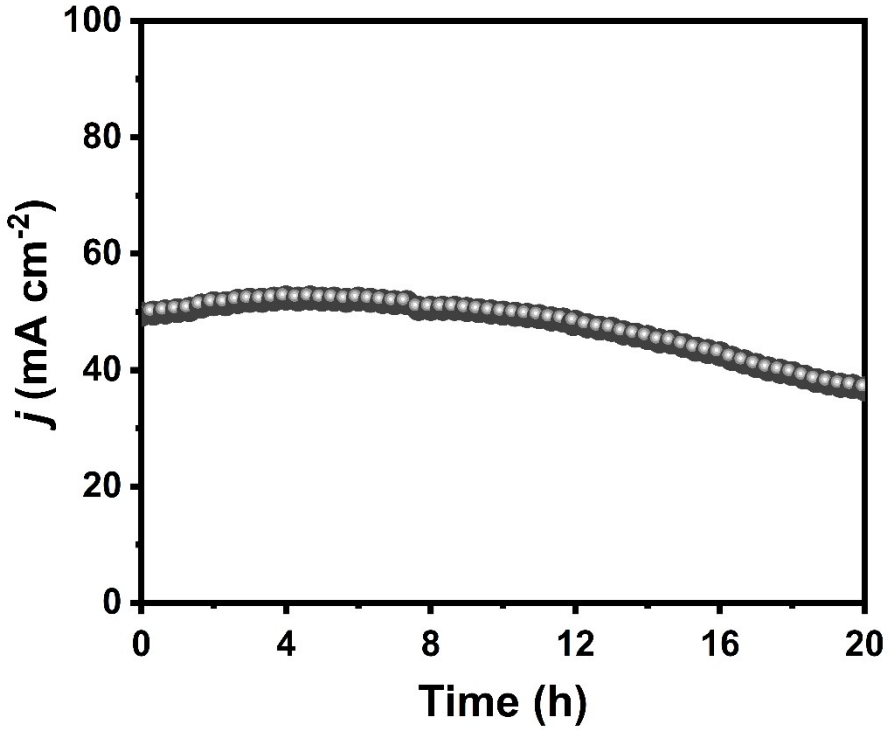

Figure S25. The long-term stability test of Pt/C in OHzS system.

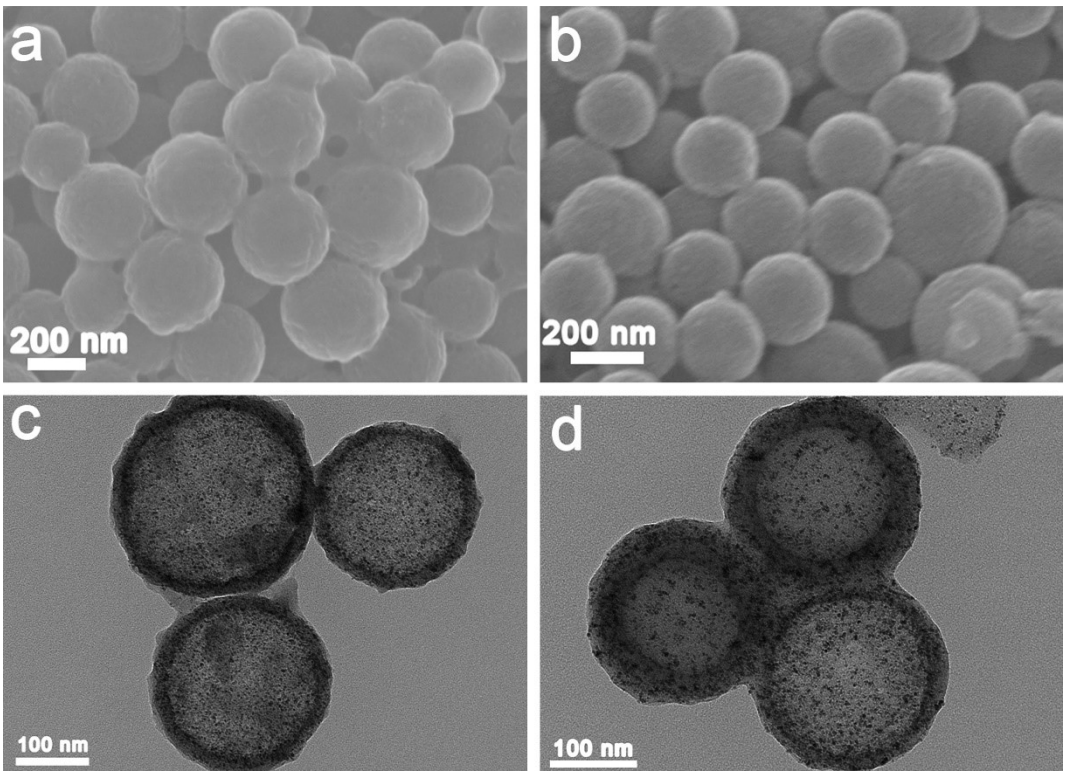

Figure S26. The structure characterizations of Ru/NSCS after durability investigation. (a, b) SEM images after HER and HzOR, respectively; (c, d) TEM images after HER and HzOR, respectively.

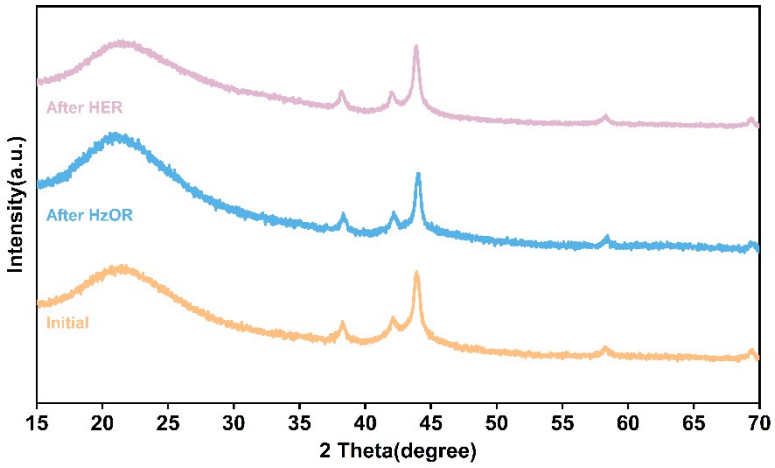

Figure S27. The compared XRD patterns of Ru/NSCS after HER and HzOR electrolysis, respectively.

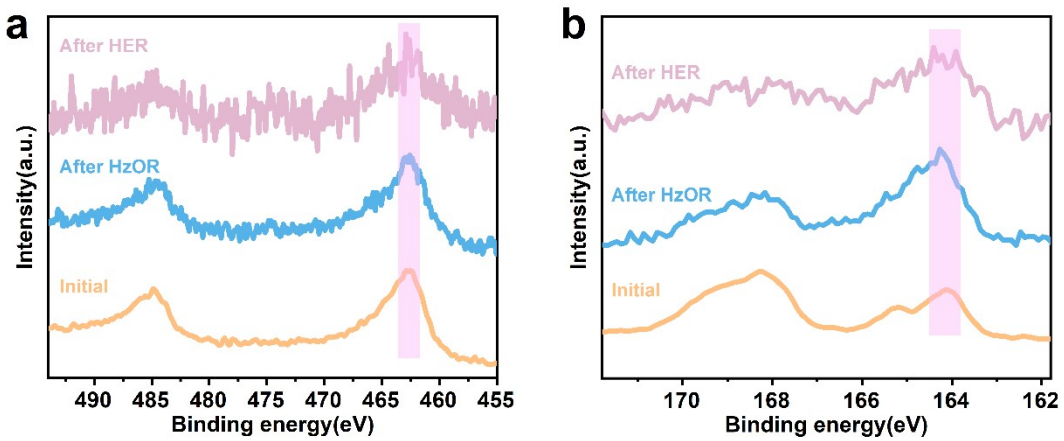

Figure S28. The compared high-resolution XPS spectra of Ru/NSCS after durability investigation. High-resolution XPS spectra of Ru 3p (a) and S 2p (b).

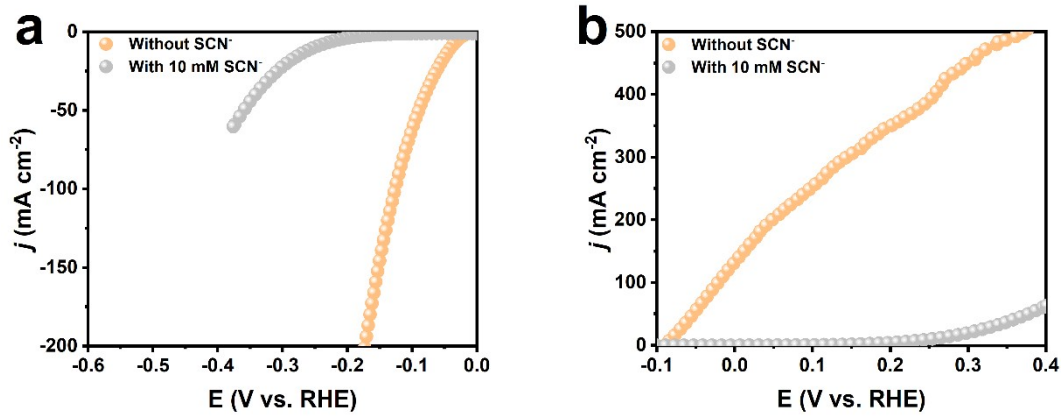

Figure S29. LSV curves of Ru/NSCS for (a) HER and (b) HzOR with and without 10 mM KSCN.

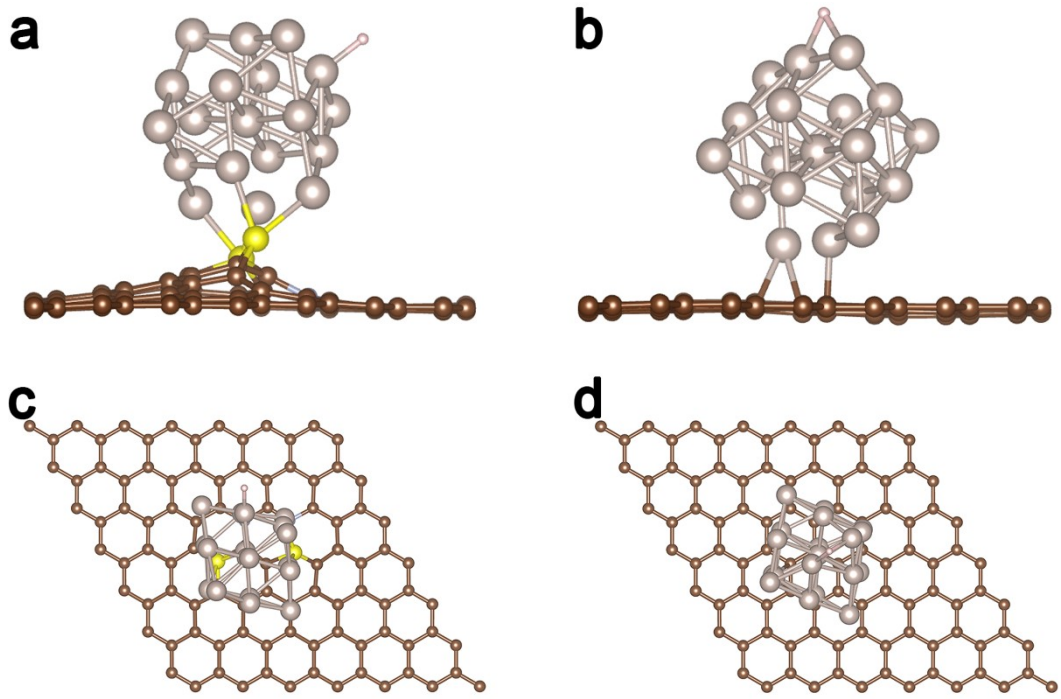

Figure S30. The adsorption model of intermediate *H. (a) Side view on Ru/NSCS; (b) Side view on Ru/CS; (c) Top view on Ru/NSCS; (d) Top view on Ru/CS. The pink, silver, brown, yellow, and blue balls represent H, Ru, C, S and N atoms, respectively.

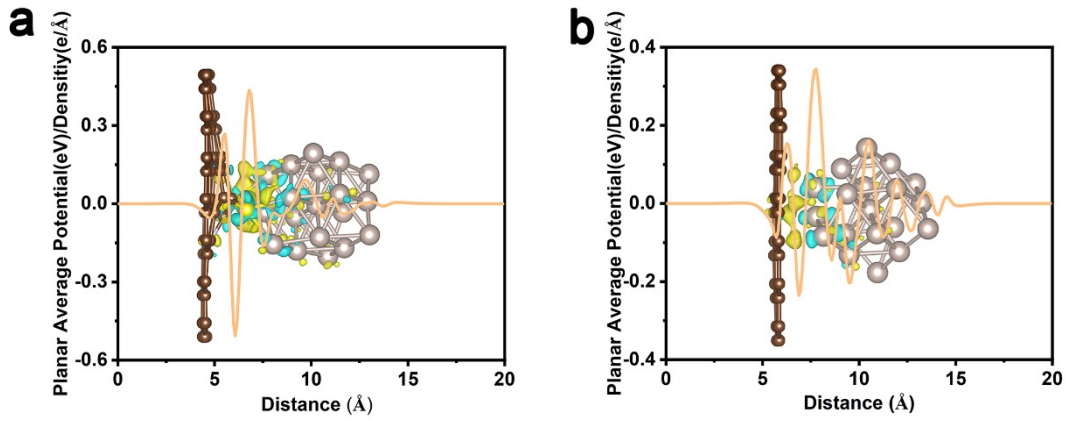

Figure S31. The charge density difference and planar-averaged electron density difference of (a) Ru/NSCS and (b) Ru/CS. The yellow and cyan colors indicate charge accumulation and depletion, respectively. The isovalues are 0.003 eÅ^{-3}.

Table S1. EA results of the as-prepared sample.

	N contents (wt%)	S contents (wt%)
Ru/NSCS	**1.150**	**3.351**

Table S2. Comparison of the electrocatalytic activities of Ru/NSCS with other reported materials for HER. η_{10} is the HER overpotential corresponding to 10 mA cm^{-2}.

Materials	Electrolyte	η_{10} (mV)	Tafel slope (mV dec^{-1})	References
Ru/NSCS	**1 M KOH**	**40**	**36.7**	**This work**
RP-CPM	1 M KOH	24	47.3	11
PW-Co_3N NWA/NF	1 M KOH	41	40	8
Ru-Ru_2PΦNPC	1 M KOH	46	39.75	15
Ru@CN	1 M KOH	32	53	16
RuP/C-PAN	1 M KOH	28	30	17
S-RuP@NPSC	1 M KOH	92	90.23	18
Ru–S/N–C	1 M KOH	10	36	19
Ru/MPNC	1 M KOH	13	30	20
Ru/Co@OG	1 M KOH	13	22.8	21

Table S3. Comparison of the electrocatalytic activities of Ru/NSCS with other reported materials for HzOR. η_{10} is the HzOR overpotential corresponding to 10 mA cm^{-2}.

Materials	Electrolyte	η_{10} (mV)	Tafel slope (mV dec^{-1})	References
Ru/NSCS	1 M KOH+0.4 M N_2H_4	-81	33.8	This work
RP-CPM	1 M KOH+0.3 M N_2H_4	-70	47.6	11
PW-Co_3N NWA/NF	1 M KOH+0.1 M N_2H_4	-55	14	8
CC@WS_2/Ru-450	1 M KOH+0.5 M N_2H_4	-74	42.2	22
p-Co/CF	1 M KOH+0.5 M N_2H_4	-150	8.83	23
RuP/C-PAN	1 M KOH+0.3 M N_2H_4	-101	30	17
Au1Pt8	1 M KOH+0.5 M N_2H_4	502	60	24
CC@WO_3/Ru-450	1 M KOH+0.5 M N_2H_4	-58	/	25
Ni NCNA	1 M KOH+0.3 M N_2H_4	-26	32.6	26
Ni_3N-Co_3N	1 M KOH+0.1 M N_2H_4	-88	21.6	10

Table S4. Comparison of the electrocatalytic activities of Ru/NSCS with other reported materials for OHzS. E_{10} is the working voltage corresponding to the current density of 10 mA cm^{-2} in the two-electrode system.

Materials	Electrolyte	E_{10}	References
Ru/NSCS	1 M KOH+0.4 M N_2H_4	26	This work
RP-CPM	1 M KOH+0.3 M N_2H_4	23	11
PW-Co_3N NWA/NF	1 M KOH+0.1 M N_2H_4	28	8
CC@WS_2/Ru-450	1 M KOH+0.5 M N_2H_4	15.4	22
RuP/C-PAN	1 M KOH+0.3 M N_2H_4	30	17
Au1Pt8	1 M KOH+0.5 M N_2H_4	172	24
CC@WO_3/Ru-450	1 M KOH+0.5 M N_2H_4	25	25
Ni NCNA	1 M KOH+0.3 M N_2H_4	23	26
Ru/MPNC	1 M KOH+0.5 M N_2H_4	41	20

Notes and references

1 G. Kresse and D. Joubert, *Phys. Rev. B.*, 1999, **59**, 1758.

2 G. Kresse and J. Hafner, *Phys. Rev. B.*, 1993, **47**, 558.

3 G. Kresse and J. Furthmuller, *Phys. Rev. B.*, 1996, **54**, 11169.

4 J. P. Perdew, K. Burke and M. Ernzerhof, *Phys. Rev. Lett.*, 1996, **77**, 3865.

5 D. Bumüller, A.-S. Hehn, E. Waldt, R. Ahlrichs, M. M. Kappes and D. Schooss, *J. Phys. Chem. C.*, 2016, **121**, 10645-10652.

6 H. J. Monkhorst and J. D. Pack, *Phys. Rev. B.*, 1976, **13**, 5188.

7 J. K. Nørskov, J. Rossmeisl, A. Logadottir, L. Lindqvist, J. R. Kitchin, T. Bligaard and H. Jónsson, *J. Phys. Chem. B.*, 2004, **108**, 17886-17892.

8 Y. Liu, J. Zhang, Y. Li, Q. Qian, Z. Li, Y. Zhu and G. Zhang, *Nat. Commun.*, 2020, **11**, 1853.

9 J. Zhang, Y. Liu, J. Li, X. Jin, Y. Li, Q. Qian, Y. Wang, A. EI-Harairy, Z. Li, Y. Zhu, H. Zhang, M. Cheng, S. Zen and G. Zhang, *ACS Appl. Mater. Interfaces.*, 2021, **13**, 3881-3890.

10 Q. Qian, J. Zhang, J. Li, Y. Li, X. Jin, Y. Zhu, Y. Liu, Z. Li, A. EI‐Harairy, C. Xiao, G. Zhang and Y. Xie, *Angew. Chem. Int. Ed.*, 2021, **60**, 5984-5993.

11 Y. Li, J. Zhang, Y. Liu, Q. Qian, Z. Li, Y. Zhu and G. Zhang, *Sci. Adv.*, 2020, **6**, eabb4197.

12 Computational Chemistry Comparison and Benchmark Database. http://cccbdb.nist.gov/.

13 M. Yu and D. R. Trinkle, *J. Chem. Phys.*, 2011, **134**, 064111.

14 W. Tang, E. Sanville and G. Henkelman, *J. Phys. Condens. Matter.*, 2009, **21**, 084204.

15 J. Yu, G. Li, H. Liu, L. Zhao, A. Wang, Z. Liu, H. Li, H. Liu, Y. Hu and W. Zhou, *Adv. Funct. Mater.*, 2019, **29**, 1901154.

16 X. F. Lu, L. Yu and X. W. Lou, *Sci. Adv.*, 2019, **5**, eaav6009.

17 Q. Qian, W. Wang, G. Wang, X. He, Y. Feng, Z. Li, Y. Zhu, Y. Zhang and G. Zhang, *Small*, 2022, **18**, 2200242.

18 X. Liu, F. Liu, J. Yu, G. Xiong, L. Zhao, Y. Sang, S. Zuo, J. Zhang, H. Liu and W. Zhou, *Adv. Sci.*, 2020, **7**, 2001526.

19 C. Li, J. Zhao, L. Xie, Y. Wang, H. Tang, L. Zheng and G. Li, *J. Mater. Chem. A.*, 2021, **9**, 12659-12669.

20 J. Wang, X. Guan, H. Li, S. Zeng, R. Li, Q. Yao, H. Chen, Y. Zheng and K. Qu, *Nano Energy*, 2022, **100**, 107467.

21 P. Su, W. Pei, X. Wang, Y. Ma, Q. Jiang, J. Liang, S. Zhou, J. Zhao, J. Liu and G.Q.M. Lu, *Angew. Chem. Int. Ed.*, 2021, **60**, 16044-16050.

22 J. Li, Y. Li, J. Wang, C. Zhang, H. Ma, C. Zhu, D. Fan, Z. Guo, M. Xu, Y. Wang and H. Ma, *Adv. Funct. Mater.*, 2022, **32**, 2109439.

23 Q. Liu, X. Liao, Y. Tang, J. Wang, X. Lv, X. Pan, R. Lu, Y. Zhao, X. Yu and H. Wu, *Energy & Environ. Sci.*, 2022, **15**, 3246-3256.

24 Y. Yu, S. Lee, J. Theerthagiri, Y. Lee and M.Y. Choi, *Appl. Catal. B. Environ.*, 2022, **316**, 121603.

25 J. Li, C. Zhang, C. Zhang, H. Ma, Y. Yang, Z. Guo, Y. Wang and H. Ma, *Chem. Eng. J.*, 2022, **430**, 132953.

26 Y. Li, J. Li, Q. Qian, X. Jin, Y. Liu, Z. Li, Y. Zhu, Y. Guo and G. Zhang, *Small*, 2021, **17**, 2008148.